

# Photocatalytic conversion of carbon dioxide to methanol over different precursors of graphitic carbon nitride supported on fibrous silica iron

Anwar Johari<sup>1,2\*</sup>, Nurul Sahida Hassan<sup>2</sup> and Norain Zulkifli<sup>2</sup>

<sup>1</sup>Centre of Hydrogen Energy, Institute of Future Energy, Universiti Teknologi Malaysia, 81310 UTM Johor Bahru, Johor, Malaysia.

<sup>2</sup>Faculty of Chemical and Energy Engineering, Universiti Teknologi Malaysia, 81310 UTM Johor Bahru, Johor, Malaysia.

**Abstract.** In this study, the graphitic carbon nitride ( $g\text{-C}_3\text{N}_4$ ) was successfully synthesized through thermal polymerization under three different  $g\text{-C}_3\text{N}_4$  precursors such as urea ( $U\text{-}g\text{-C}_3\text{N}_4$ ), melamine ( $M\text{-}g\text{-C}_3\text{N}_4$ ) and dicyandiamide ( $D\text{-}g\text{-C}_3\text{N}_4$ ) and then doped into the fibrous silica iron (FSFe), denoted as  $U\text{-}g\text{-C}_3\text{N}_4/\text{FSFe}$ ,  $M\text{-}g\text{-C}_3\text{N}_4/\text{FSFe}$ , and  $D\text{-}g\text{-C}_3\text{N}_4/\text{FSFe}$ , respectively. The synthesized catalysts were characterized using X-ray Diffraction (XRD), Fourier Transform Infrared Spectrometer (FTIR), and UV-Vis Diffuse Reflectance Spectroscopy (UV-Vis/DRS) and also tested for photocatalytic conversion of carbon dioxide ( $\text{CO}_2$ ) to methanol ( $\text{CH}_3\text{OH}$ ). The study indicated that altering the precursors had a substantial impact on the physicochemical features of the FSFe, which in turn increased the catalytic performance of the conversion of  $\text{CO}_2$  to  $\text{CH}_3\text{OH}$ .  $U\text{-}g\text{-C}_3\text{N}_4/\text{FSFe}$  exhibits the highest  $\text{CH}_3\text{OH}$  yield ( $2.3 \times 10^4 \mu\text{mol g}_{\text{cat}}^{-1}$ ) compared to bare FSFe,  $D\text{-}g\text{-C}_3\text{N}_4/\text{FSFe}$  and  $M\text{-}g\text{-C}_3\text{N}_4/\text{FSFe}$  under visible light irradiation within 240 min. The higher  $\text{CH}_3\text{OH}$  yield over  $U\text{-}g\text{-C}_3\text{N}_4/\text{FSFe}$  is mostly owing to the lower bandgap energy of  $U\text{-}g\text{-C}_3\text{N}_4/\text{FSFe}$ , as well as the advantageous interaction between  $g\text{-C}_3\text{N}_4$  and FSFe.

## 1 Introduction

Carbon dioxide ( $\text{CO}_2$ ) is the primary contributor to greenhouse effects, stemming from both natural and artificial processes. It's acknowledged that  $\text{CO}_2$  is essential for plant growth and various industrial applications [1]. However, it's imperative to maintain a balance between  $\text{CO}_2$  emissions and consumption to preserve environmental stability. In reality, human industrial activities result in higher  $\text{CO}_2$  emissions than consumption, disrupting the  $\text{CO}_2$  equilibrium and exacerbating global warming [2]. To address this issue, numerous researchers have conducted studies. One potential solution is the conversion of  $\text{CO}_2$  into valuable low-carbon fuels, such as methanol [3, 4].

In recent years, electrochemical catalyst approaches for  $\text{CO}_2$  conversion have garnered significant attention due to their numerous advantages [5]. Nevertheless, the kinetics of  $\text{CO}_2$  electroreduction remain suboptimal, even with high electrode reduction potential and the application of electrocatalysts. Another viable approach to converting  $\text{CO}_2$  into methanol involves chemical, photochemical, photoelectrochemical, and photocatalytic reduction methods. Among these, photocatalytic conversion of  $\text{CO}_2$  has been favored due to its high conversion efficiency, straightforward conversion procedures, and reasonable production cost [6]. In this process, a photocatalyst enhances  $\text{CO}_2$  reduction by absorbing light, raising it to a higher energy level, and

transferring this energy to a reacting substance to facilitate a chemical reaction [4].

In response to the escalating global environmental challenges, there is a strong need to develop efficient, cost-effective photocatalysts that are responsive to visible light for converting  $\text{CO}_2$ . A wide range of semiconductor materials, including titanium dioxide, zinc oxide, zirconium dioxide, iron oxide, graphitic carbon nitride ( $g\text{-C}_3\text{N}_4$ ), and transition metal complexes, have been extensively studied for the photocatalytic conversion of  $\text{CO}_2$  [3, 7, 8]. Among these,  $g\text{-C}_3\text{N}_4$  has gained prominence as a highly promising photocatalytic material in recent years for  $\text{CO}_2$  reduction under solar light exposure [9]. This is attributed to its affordability, unique chemical stability, environmentally friendly nature, and tunable microstructure [10].

Interestingly,  $g\text{-C}_3\text{N}_4$  remains stable when exposed to light in both acidic and basic aqueous solutions due to the strong covalent bonds between carbon and nitrogen atoms [11]. It possesses an energy bandgap of 2.7 eV and can absorb the solar spectrum with a wavelength of less than 420 nm [12]. The  $g\text{-C}_3\text{N}_4$  structure features interlayers with either a  $\text{C}_3\text{N}_3$  ring or a  $\text{C}_6\text{N}_7$  ring, and the graphite framework maintains a spacing of 0.326 nm between the two layers. These rings are connected by the N atom's tail, forming an uninterrupted layer with planar extension.

\* Corresponding author: [anwar@utm.my](mailto:anwar@utm.my)

Various synthesis methods, including thermal polymerization, solvent hot techniques, template-directed solid-state, soft-templating synthesis, and sonochemical processes, have been commonly employed to produce g-C<sub>3</sub>N<sub>4</sub> [13]. However, its limited surface area (10 m<sup>2</sup> g<sup>-1</sup>) and relatively low photocatalytic efficiency have made it less than ideal as a photocatalyst. Consequently, researchers have explored techniques such as coupling with other semiconductors or introducing co-catalysts to enhance the performance of g-C<sub>3</sub>N<sub>4</sub>. Moreover, the improved photocatalytic activity is associated with the specific structure resulting from different heat treatment temperatures, the quantity of g-C<sub>3</sub>N<sub>4</sub>, broad optical absorption range, effective separation and transport of electronic holes, and the composition of composite materials [14].

Numerous studies have investigated the synthesis of co-catalysts in conjunction with g-C<sub>3</sub>N<sub>4</sub>, but there has been a limited comparison of these synthesis methods. Common nitrogenous precursors include urea, dicyandiamide, and melamine, each having distinct structural characteristics. In this study, we opted for these structurally diverse nitrogenous precursors to produce g-C<sub>3</sub>N<sub>4</sub> through fractional thermal polymerization, with the aim of conducting a comprehensive examination of the resulting g-C<sub>3</sub>N<sub>4</sub> structures and properties. Finally, the synthesized g-C<sub>3</sub>N<sub>4</sub> materials were doped into fibrous silica iron and assessed for their efficacy in the photocatalytic conversion of CO<sub>2</sub> to methanol.

## 2 Materials and methods

### 2.1 Materials

The chemicals used in the experiment were tetraethyl orthosilicate (TEOS), cetyltrimethylammonium bromide (CTAB), butanol, urea, toluene, commercial iron oxide, Urea, melamine and which were purchased from Sigma-Aldrich, Malaysia. Other than that, the all reagents were prepared using deionized water.

### 2.2 Catalyst preparation

Graphitic carbon nitride was synthesized by using different type of precursors which is urea, dicyandiamide and melamine. In this study, for synthesis of g-C<sub>3</sub>N<sub>4</sub> nanomaterial, 1 g of urea, dicyandiamide and melamine were put into a ceramic crucible separately. Then all the precursors in each crucible were calcined for 30 min at 620 °C/min under muffle furnace. The polymeric catalyst was then cooled to room temperature. In order to produce fine powder, the result of catalyst obtained was crushed for further purpose. Consequently, the resultant g-C<sub>3</sub>N<sub>4</sub> obtained by urea, dicyandiamide and melamine precursors were denoted as U-gC<sub>3</sub>N<sub>4</sub>, D-gC<sub>3</sub>N<sub>4</sub> and M-gC<sub>3</sub>N<sub>4</sub>, respectively.

Fibrous silica iron (FSFe) was synthesized by using microemulsion technique together with crystal-seed crystallization method. Firstly, 24.65 g of CTAB and 14.72 g of urea were mixed in 732 mL of distilled water,

stirred for 5 min at vigorous stirring which is 850 rpm. Next, 624 mL of toluene and 37 mL of 1-butanol were added into the mixture and stirred for another 15 min at room temperature. After that, 3 g of iron seed was added into the mixture and stirred for another 30 min. Subsequently, 56 mL of TEOS was added drop wise and the mixture was stirred for 2 hours at room temperature. After 2 hours stirring, the resulting mixture was heated in oven for 6 hours at 120 °C. The heated product was dried overnight at 110 °C before calcination at 550 °C for 6 hours. A dry brown solid catalyst was obtained and it represented FSFe catalyst.

The preparation steps for g-C<sub>3</sub>N<sub>4</sub>/FSFe catalysts was started with dissolving 0.05 g of g-C<sub>3</sub>N<sub>4</sub> from different precursor and 0.95 g of FSFe into 50mL distilled water. Then, the mixture was stirred for 30 min and then dried in oven at 110 °C overnight. Next, the mixture was transferred into microwave for 30 min at 450 W. Consequently, the resultant g-C<sub>3</sub>N<sub>4</sub>/FSFe obtained by urea, dicyandiamide and melamine precursors were denoted as U-gC<sub>3</sub>N<sub>4</sub>/FSFe, D-gC<sub>3</sub>N<sub>4</sub>/FSFe and M-gC<sub>3</sub>N<sub>4</sub>/FSFe respectively.

### 2.3 Characterization

The catalysts crystallinity were verified by D8 ADVANCE Bruker X-ray diffractometer. Meanwhile, the chemical properties of the catalysts was detected by the KBr method via Perkin Elmer Spectrum GX FT-IR. The optical properties of the catalyst were measured by using Agilent Technologies Cary 60 UV-Vis spectrometer with an integrating sphere.

### 2.4 Photocatalytic measurement

An amount of photocatalyst (0.06 g L<sup>-1</sup>) was dispersed into 100 mL solution CO<sub>2</sub> which consist of distilled water and TEA (sacrificial agent). The photocatalytic conversion of CO<sub>2</sub> was conducted using a fixed batch reactor with a cooling system CO<sub>2</sub> was fed into the slurry photoreactor through a gas inlet pipe at the top. A 39 W metal halide lamp with a wavelength of 400 nm was used for visible light source. The solution was stirred in a dark for 60 min to achieve absorption equilibrium and then exposed under visible light for another 4 hours. The absorption equilibrium was determined by conducting a reaction in the dark for 60 min. During the process, 1 mL of solution sample was collected using a syringe for every 60 min in the dark and in every 30 min under visible light and then, centrifuged using Beckman Coulter Microfuge 16 Centrifuge at 14,000 rpm for 5 min. Then, the concentration of methanol was analyzed using Gas chromatography (GC) at the area peak of methanol 1.036.

## 3 Results and discussion

### 3.1 Crystallinity studies

The XRD patterns of the synthesized catalyst in the range of 2θ=10-80° are shown in Figure 1. Several peaks

at  $2\theta = 24.19^\circ, 30.03^\circ, 33.07^\circ, 35.50^\circ, 40.84^\circ, 43.30^\circ, 49.57^\circ, 53.89^\circ, 57.34^\circ$  and  $62.74^\circ$  was observed in fibrous silica iron (FSFe) corresponding to the planes (012), (220), (104), (110), (113), (202), (024), (116), (122) and (214) respectively, which attributed to the rhombohedral phase of  $\alpha\text{-Fe}_2\text{O}_3$  (ICDD card no. 33-0664) [15]. The narrow and sharp peaks were observed due to its crystalline nature, implying that the high purity of synthesized FSFe is obtained by using microemulsion method. Meanwhile, the broad peak at  $23.04^\circ$  was attributed to the amorphous silica framework of the materials [16]. For all catalyst of  $\text{g-C}_3\text{N}_4$  synthesized from different precursor doped onto FSFe show similar diffractograms, with a slight decrease in intensity, particularly for  $\text{U-gC}_3\text{N}_4/\text{FSFe}$  and  $\text{D-gC}_3\text{N}_4/\text{FSFe}$ . In contrast,  $\text{M-gC}_3\text{N}_4/\text{FSFe}$  showed the higher intensity compared to the FSFe, indicating the higher crystallinity might be due to the higher content of nitrogen [17]. Additionally, the obvious an additional peak at  $27.5^\circ$ , attributed to the (002) plane of  $\text{g-C}_3\text{N}_4$  based on the JCPDS no.87-1526 [11].

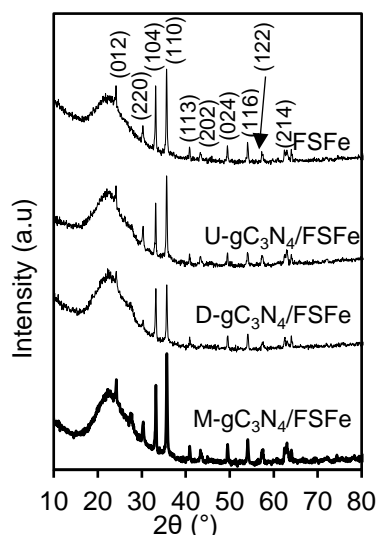


**Fig. 1.** XRD patterns of the FSFe and  $\text{g-C}_3\text{N}_4/\text{FSFe}$  under different precursors.

For chemical properties studies, all the catalysts were then characterized by FTIR and the spectra in the region of  $4000\text{-}400\text{ cm}^{-1}$  are shown in Fig. 2. Typical bands for  $\text{g-C}_3\text{N}_4$  were detected at  $806\text{ cm}^{-1}$  due to the vibration of triazine ring [18]. The  $\text{U-gC}_3\text{N}_4$  absorption band is more apparent than that of  $\text{D-gC}_3\text{N}_4$  and  $\text{M-gC}_3\text{N}_4$ , owing to its more orderly polymeric melon unit packing (Fig. 2a-c)[17]. Also, the peaks at  $1238\text{ cm}^{-1}$  and  $1322\text{ cm}^{-1}$  are related to the typical stretching vibration of C-N heterocycles [12]. Meanwhile, major absorption bands for FSFe were spotted at  $462\text{ cm}^{-1}, 800\text{ cm}^{-1}, 968\text{ cm}^{-1}, 1091\text{ cm}^{-1}$ , which were associated with the existence of M-O (M=Si and Fe), Si-OH external groups, symmetric Si-O-Si and asymmetric Si-O-Si stretching, respectively (Fig. 2d) [19]. The intensity of Si-O-Si bonds of FSFe was seems decreased when incorporation of  $\text{g-C}_3\text{N}_4$ , suggesting that Si-O-Si were isomorphously with C and N elements to form Si-O-C and Si-O-N, respectively. This result showed there is an interaction between  $\text{g-C}_3\text{N}_4$  with  $\text{SiO}_2$ . Interestingly, the

obvious peaks at  $1322$  and  $1238\text{ cm}^{-1}$  corresponding to the C-N heterocycles was observed in the  $\text{U-gC}_3\text{N}_4$ , may be due to its orderly polymeric melon unit packing compared another precursor of  $\text{g-C}_3\text{N}_4$ .

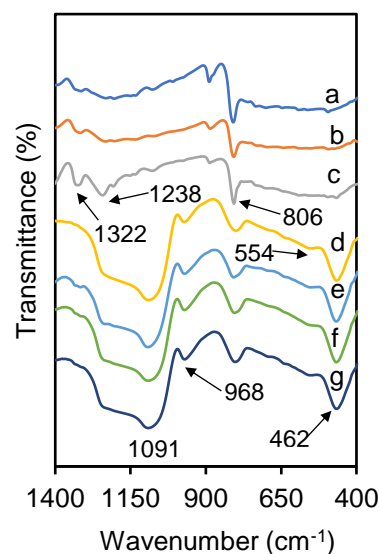


**Fig. 2.** FTIR spectra of (a)  $\text{U-gC}_3\text{N}_4$  (b)  $\text{D-gC}_3\text{N}_4$  (c)  $\text{M-gC}_3\text{N}_4$  (d) FSFe (e)  $\text{U-gC}_3\text{N}_4/\text{FSFe}$  (f)  $\text{D-gC}_3\text{N}_4/\text{FSFe}$  (g)  $\text{M-gC}_3\text{N}_4/\text{FSFe}$

The optical behavior of photocatalysts results in an important impact on photocatalytic reactions. The UV-Vis's spectra for all photocatalysts was recorded in the spectral range  $200\text{-}800\text{ nm}$  to investigate the optical properties of the catalyst as illustrated in Fig. 3. The bandgap of the samples was calculated using the equation of  $E=1240/\lambda$  where  $E$  is the band gap energy in eV and  $\lambda$  is the wavelength in nanometres.

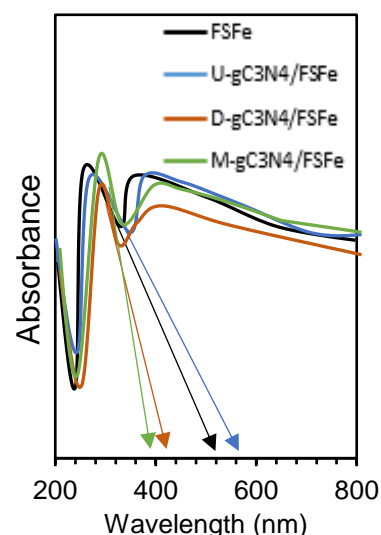


**Fig. 3.** UV-Vis's spectra of all catalysts.

As seen, the absorption edges reached over  $400\text{ nm}$ , indicating that all the synthesized catalyst could responds to the visible light. The summary of the band gap for all catalysts are stated in Table 1. The band gap energy of FSFe is  $2.38\text{ eV}$ , and it altered the band gap

energy when g-C<sub>3</sub>N<sub>4</sub> doped on FSFe. The band gap energy of D-gC<sub>3</sub>N<sub>4</sub>/FSFe (2.95 eV) and M-gC<sub>3</sub>N<sub>4</sub>/FSFe (3.18 eV) is higher compared to the FSFe, may be due to the quantum confinement effect [13]. Likewise, the U-gC<sub>3</sub>N<sub>4</sub>/FSFe (2.21 eV) showed the lowest bandgap among all catalyst. This result led to the potential use of it in visible light responsive photocatalytic reaction as the photogenerated electrons and holes were effectively separated due to lower bandgap, thus possibly induced charge-transfer transition between FSFe species and g-C<sub>3</sub>N<sub>4</sub>.

**Table 1** Band gap energy of the catalyst

Catalyst	Bandgap (eV)
FSFe	2.38
U-gC <sub>3</sub> N <sub>4</sub> /FSFe	2.21
D-gC <sub>3</sub> N <sub>4</sub> /FSFe	2.95
M-gC <sub>3</sub> N <sub>4</sub> /FSFe	3.18

The performance of the synthesized catalyst towards on the photoconversion of CO<sub>2</sub> to methanol was illustrated in Fig. 4, which the reaction was conducted under the visible light irradiation. As seen, U-gC<sub>3</sub>N<sub>4</sub>/FSFe exhibits the highest performance (2.3 x 10<sup>4</sup> μmol g<sub>cat</sub><sup>-1</sup>) compared to bare FSFe, D-gC<sub>3</sub>N<sub>4</sub>/FSFe and M-gC<sub>3</sub>N<sub>4</sub>/FSFe. The reason might be due to the lowest bandgap energy of U-gC<sub>3</sub>N<sub>4</sub>/FSFe. Notably, the interaction between g-C<sub>3</sub>N<sub>4</sub> and FSFe could improve the generation of g-C<sub>3</sub>N<sub>4</sub> and FSFe heterojunction in U-gC<sub>3</sub>N<sub>4</sub>/FSFe. Furthermore, the CH<sub>3</sub>OH yield for all catalysts appears to be steady after 180 minutes, which can be attributed to the equal rates obtained between CH<sub>3</sub>OH formation and CH<sub>3</sub>OH re-oxidation.

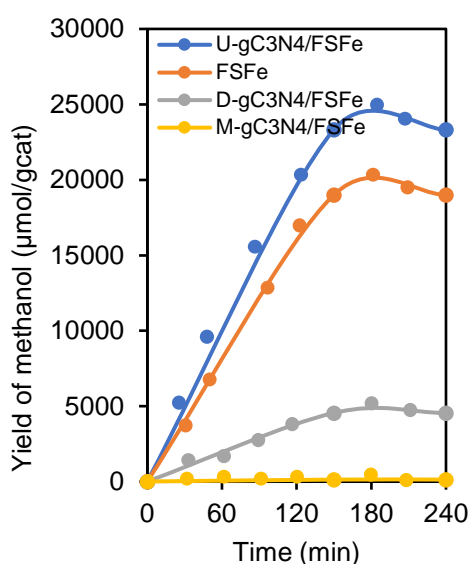


**Fig. 4.** Catalytic performance of the catalyst towards conversion of CO<sub>2</sub> to methanol.

## 4 Conclusion

In this study, three different precursors of g-C<sub>3</sub>N<sub>4</sub> which is urea, melamine and dicyandiamide were used to

prepare the g-C<sub>3</sub>N<sub>4</sub> by thermal polymerization, and denoted as U-gC<sub>3</sub>N<sub>4</sub>, M-gC<sub>3</sub>N<sub>4</sub> and D-gC<sub>3</sub>N<sub>4</sub>, respectively. The resulting materials were then doped into fibrous silica iron (FSFe), designated as U-gC<sub>3</sub>N<sub>4</sub>/FSFe, M-gC<sub>3</sub>N<sub>4</sub>/FSFe, and D-gC<sub>3</sub>N<sub>4</sub>/FSFe, respectively. The synthesised catalysts were evaluated for their ability to photocatalytically convert CO<sub>2</sub> to CH<sub>3</sub>OH. According to the research, changing the precursors significantly affected the physicochemical characteristics of the FSFe, which in turn improved the catalytic performance of converting CO<sub>2</sub> to CH<sub>3</sub>OH. Under visible light irradiation for 240 minutes, U-gC<sub>3</sub>N<sub>4</sub>/FSFe shows the highest CH<sub>3</sub>OH yield (2.3 x 10<sup>4</sup> μmol g<sub>cat</sub><sup>-1</sup>) when compared to bare FSFe, D-gC<sub>3</sub>N<sub>4</sub>/FSFe, and M-gC<sub>3</sub>N<sub>4</sub>/FSFe. The lower bandgap energy of U-gC<sub>3</sub>N<sub>4</sub>/FSFe and the beneficial interaction between g-C<sub>3</sub>N<sub>4</sub> and FSFe are the main causes of the greater CH<sub>3</sub>OH yield over U-gC<sub>3</sub>N<sub>4</sub>/FSFe.

The authors extend our gratitude towards Universiti Teknologi Malaysia (UTM) for the financial assistance provided through the UTM Fundamental Research (No.22H51).

## References

1. M. Aziz, A. Jalil, M. Hamid, N. Hassan, N. Khusnun, M. Bahari, A. Hatta, M. Aziz, J. Matmin, S. Zein, Lamellar-structured fibrous silica as a new engineered catalyst for enhancing CO<sub>2</sub> methanation. *Fuel*. **352**, 129113 (2023)
2. S. Chakraborty, J. Nayak, B. Ruj, P. Pal, R. Kumar, S. Banerjee, M. Sardar, P. Chakraborty, Photocatalytic conversion of CO<sub>2</sub> to methanol using membrane-integrated green approach: a review on capture, conversion and purification. *J. Environ. Chem. Eng.* **8**, 103935 (2020)
3. M. Bahari, C. Mamat, A. Jalil, L. Shing, N. Hassan, F. Aziz, M. Alhassan, M. Nawawi, K. Kidam, H. Setiabudi, Enriching the methanol generation via CO<sub>2</sub> photoconversion over the cockscomb-like fibrous silica copper. *Fuel*. **328**, 125257 (2022)
4. N. Khusnun, A. Jalil, T. Abdullah, S. Latip, C. Hitam, A. Fauzi, N. Hassan, M. Aziz, A. Rahman, F. Aziz, Influence of TiO<sub>2</sub> dispersion on silica support toward enhanced amine assisted CO<sub>2</sub> photoconversion to methanol. *J. CO<sub>2</sub> Util.* **58**, 101901 (2022)
5. A. Kaliyaperumal, P. Gupta, Y.S.S. Prasad, A.K. Chandiran, R. Chetty, Recent progress and perspective of the electrochemical conversion of carbon dioxide to alcohols. *ACS Eng. Au.* **3**, 403 (2023)
6. A. Aranda-Aguirre, J. Ojeda, J.F. de Brito, S. Garcia-Segura, M.V.B. Zaroni, H. Alarcon, Photoelectrodes of Cu<sub>2</sub>O with interfacial structure of topological insulator Bi<sub>2</sub>Se<sub>3</sub> contributes to selective photoelectrocatalytic reduction of CO<sub>2</sub> towards methanol. *J. CO<sub>2</sub> Util.* **39**, 101154 (2020)
7. Q. Mou, Z. Guo, Y. Chai, B. Liu, C. Liu, Visible light assisted production of methanol from CO<sub>2</sub> using CdS@CeO<sub>2</sub> heterojunction. *J. Photochem. Photobiol.* **219**, 112205 (2021)

8. H. Zhao, F. Pan, Y. Li, A review on the effects of TiO<sub>2</sub> surface point defects on CO<sub>2</sub> photoreduction with H<sub>2</sub>O. *J. Materiomics*. **3**, 17 (2017)
9. H. Zhang, X. Ren, B. Zhang, A. Jia, Y. Wang, Size effect of Cu nanoparticles in Cu/g-C<sub>3</sub>N<sub>4</sub> composites on properties for highly efficient photocatalytic reduction of CO<sub>2</sub> to methanol. *ACS Appl. Mater. Interfaces*. **15**, 53515 (2023)
10. P. Ganji, R.K. Chowdari, B. Likozar, Photocatalytic reduction of carbon dioxide to methanol: carbonaceous materials, kinetics, industrial feasibility, and future directions. *Energy Fuels*. **37**, 7577 (2023)
11. M. Azami, A. Jalil, N. Hassan, I. Hussain, A. Fauzi, M. Aziz, Green carbonaceous material–fibrous silica-titania composite photocatalysts for enhanced degradation of toxic 2-chlorophenol, *J. Hazard. Mater.* **414**, 125524 (2021)
12. M. Azami, A. Jalil, C. Hitam, N. Hassan, C. Mamat, R. Adnan, N. Chanlek, Tuning of the electronic band structure of fibrous silica titania with g-C<sub>3</sub>N<sub>4</sub> for efficient Z-scheme photocatalytic activity. *Appl. Surf. Sci.* **512**, 145744 (2020)
13. V. Ragupathi, P. Panigrahi, N.G. Subramaniam, Bandgap engineering in graphitic carbon nitride: Effect of precursors. *Optik*. **202**, 163601 (2020)
14. A. Kumar, P. Raizada, V.K. Thakur, V. Saini, A.A.P. Khan, N. Singh, P. Singh, An overview on polymeric carbon nitride assisted photocatalytic CO<sub>2</sub> reduction: strategically manoeuvring solar to fuel conversion efficiency. *Chem. Eng. Sci.* **230**, 116219 (2021)
15. M.I. Rahmah, R.S. Sabry, W.J. Aziz, Preparation and photocatalytic property of Fe<sub>2</sub>O<sub>3</sub>/ZnO composites with superhydrophobicity, *Int. J. Miner. Metall. Mater.* **28**, 1072 (2021).
16. N. Hassan, A. Jalil, I. Fei, M. Razak, N. Khusnun, M. Bahari, Y. Riwayati, S. Suprpto, D. Prasetyoko, M. Firmansyah, Vanadia as an electron-hole recombination inhibitor on fibrous silica-titania for selective hole oxidation of ciprofloxacin and Congo red photodegradation, *Chemosphere*. **338**, 139502 (2023)
17. Z. Zhao, Y. Ma, J. Fan, Y. Xue, H. Chang, Y. Masubuchi, S. Yin, Synthesis of graphitic carbon nitride from different precursors by fractional thermal polymerization method and their visible light induced photocatalytic activities. *J. Alloys Compd.* **735**, 1297 (2018)
18. J. Gao, Y. Wang, S. Zhou, W. Lin, Y. Kong, A facile one-step synthesis of Fe-doped g-C<sub>3</sub>N<sub>4</sub> nanosheets and their improved visible-light photocatalytic performance. *ChemCatChem*. **9**, 1708 (2017)
19. N. Hassan, A. Jalil, L. Twu, N. Fatah, H. Hambali, I. Hussain, M. Firmansyah, Hydroisomerization of n-hexane over metal oxides-loaded fibrous silica catalyst for cleaner fuel production. *Int. J. Hydrogen Energy*. **48**, 20525 (2023)